

Limits for quantum networks with semiconductor entangled photon sources

Jingzhong Yang,^{1,*} Michael Zopf,^{1,*} Pengji Li,^{1,*} Nand Lal Sharma,² Weijie Nie,² Frederik Benthin,¹ Tom Fandrich,¹ Eddy Patrick Rugeramigabo,¹ Caspar Hopfmann,² Robert Keil,^{2,†} Oliver G. Schmidt,^{2,3,4} and Fei Ding^{1,‡}

¹*Institut für Festkörperphysik, Leibniz Universität Hannover, Appelstraße 2, 30167 Hannover, Germany*

²*Institute for Integrative Nanosciences, Leibniz IFW Dresden, Helmholtzstraße 20, 01069 Dresden, Germany*

³*Material Systems for Nanoelectronics, Technische Universität Chemnitz, 09107 Chemnitz, Germany*

⁴*Nanophysics, Faculty of Physics and Würzburg-Dresden Cluster of Excellence ct.qmat, TU Dresden, 01062 Dresden, Germany*

(Dated: September 15, 2021)

Semiconductor quantum dots are promising constituents for future quantum communication. Although deterministic, fast, efficient, coherent, and pure emission of entangled photons has been realized, implementing a practical quantum network remains outstanding. Here we explore the limits for sources of polarization-entangled photons from the commonly used biexciton-exciton cascade. We stress the necessity of tuning the exciton fine structure, and explain why the often observed time evolution of photonic entanglement in quantum dots is not applicable for large quantum networks. The consequences of device fabrication, dynamic tuning techniques and statistical effects for practical network applications are investigated. We identify the critical device parameters and present a numerical model for benchmarking the device scalability in order to bring the realization of distributed semiconductor-based quantum networks one step closer to reality.

I. INTRODUCTION

Entanglement is a fundamental resource in next-generation quantum technologies such as quantum communication [1–3] or quantum computing [4]. The efficient distribution of entanglement between remote parties is a key-enabling element for the realization of a global quantum internet [5, 6]. Photons are considered the best "flying" quantum bits for this goal since they can travel long distances with high resistance to decoherence from the environment [7, 8]. Quantum information is encoded on the light by means of observables with continuous [9] or discrete eigenvalues [10]. The polarization degree of single photons has been utilized to transfer quantum states via optical fiber [11] or satellite signals [12]. However, the employed sources of single photons and polarization-entangled photon pairs are based on spontaneous parametric down-conversion (SPDC) [13, 14], a probabilistic process comprising a fundamental efficiency limit impeding practical application [15, 16].

Self-assembled semiconductor QDs (QDs) have been studied extensively in the last decades and have become promising candidates for the generation of single photons [17, 18], entangled pairs [19, 20], or linear cluster states [21]. They can also serve as local nodes for storing quantum information (storage/coherence times up to 1 ms [22]). However, distributed quantum networks based on QDs have yet to be demonstrated. Such networks may be realized using quantum repeater schemes [23] which, among others, rely on quantum interference between photons from independent sources and entanglement swapping [24]. Photon states generated by swapping entanglement of photon pairs emitted from a single QD have been shown to violate Bells inequality [25]. The

individual properties of QDs that impact the success of entanglement swapping schemes have been well understood [26–28]. However, in the real-world application of distributed devices, it is impossible to choose the best possible values of each parameter simultaneously, since each parameter shows a statistical distribution in each device.

Here we show how the statistical distribution of QD properties limits their practical application in distributed quantum networks. Two separate dielectric antenna devices are studied, which have been reported to significantly enhance the photon extraction efficiency of QDs emitting at near-infrared [29] and telecom wavelengths [30]. The distribution of QD properties in the bare wafer and the changes induced by the device fabrication process are investigated. We discuss the necessity of tuning the exciton fine structure of each individual device for network protocols involving Bell state measurements. A suitable pair of QDs from the separate devices is tuned into resonance with each other and characterized for usability in entanglement swapping schemes [25, 31]. Polarization-entangled photon pairs are hereby generated via the biexciton-exciton (XX-X) cascade. We present a numerical model by which the entanglement swapping fidelity can be estimated based on the statistical distribution of QD parameters in each device. The presented findings shed light on the roadmap for optimizing and utilizing semiconductor photon sources in distributed quantum networks.

II. STATISTICS OF THE DEVICES

Optical quantum interference requires mode overlap of indistinguishable photons of the same wavelength. In contrast to SPDC sources, whose emission wavelength can be easily adjusted, QDs exhibit discrete spectral lines which differ from dot to dot. Therefore, the emissions have to be tuned into resonance with each other, e.g. via quantum frequency conversion [32], which is, however, limited in efficiency due to coupling and conversion losses as well as higher operation complexity. Another possibility is applying external (e.g. strain or mag-

* Contributed equally to this work

† Present address: Fraunhofer-Institut für Angewandte Festkörperphysik (IAF), Tullastraße 72, 79108 Freiburg, Germany

‡ fei.ding@fkp.uni-hannover.de

netic) fields [11, 33], for which it is important to understand the initial compatibility of two optical devices in wavelength: A too broad distribution of emission wavelengths increases the difficulty of finding similar QDs that can be tuned into resonance. Figure 1(a) shows the distribution of X emission wavelengths of two dielectric antenna devices containing GaAs/AlGaAs QDs. This virtual strain-free QD system is known for the high level of control over the optical properties, resulting in similar emission spectra and low X fine structure splittings (FSSs) [34]. Most of the QDs in the fabricated antennas emit photons at wavelengths between 773 nm and 785 nm. On the one hand, this distribution is blue-shifted and broadened comparing with the as-grown sample, which can be attributed to different local strain conditions for the QDs after device fabrication. On the other hand, both wavelength distributions are very similar, rendering the fabrication process uniform and offering a certain probability of finding a QD in each device with close-by emission wavelengths. External tuning techniques allow for tuning the emission wavelengths of QDs e.g. via temperature [35], strain [11], electric fields [36], or magnetic fields [19].

Applying external fields often result in a mutual change of parameters, as shown exemplary in fig. 1(b). Tuning the temperature from 3.4 K to 31.7 K results in a red-shift of the X emission by 0.445 nm. The temperature-induced change in the bandgap does typically not lead to changes in the X fine structure. However, increased charge fluctuations and scattering process with phonons lead to degraded first-order coherence (increased linewidths), setting a limit to the visibility for quantum interference with photons from another device. The coherence time (T_2) of the neutral X emission as a function of the temperature was obtained with a Michelson interferometer and is shown. A more than threefold decrease in coherence time is observed when tuning the temperature from 3.4 to 31.4 K. While the wavelength barely changes for low temperatures, it shifts more efficiently for a temperature greater than 15 K (fig. 1(b)).

III. NECESSITY OF FINE STRUCTURE TUNING

For experiments such as entanglement swapping with QD-based light sources, a high swapping fidelity is accomplished only if the sources emit high-fidelity entangled photon pairs themselves. In recent years it has been shown several times that high degrees of entanglement persists even with larger X fine structure splittings if one experimentally determines the phase factor for each emission [37]:

$$|\psi_{12}(t)\rangle = \frac{1}{\sqrt{2}} \left(|H_1 H_2\rangle + e^{-i\frac{S}{\hbar}t} |V_1 V_2\rangle \right) \quad (1)$$

where the phase factor is determined by the X fine structure splitting S and the time t that the exciton evolves. The distribution of the X fine structure splitting undergoes a strong change during fabrication. From fig. 2(b) it is clear that the QDs in the as-grown sample have FSSs lower than 10 μeV , much smaller than the ones in the dielectric antennas. A large FSS leads to two-photon states that oscillate between two Bell states with

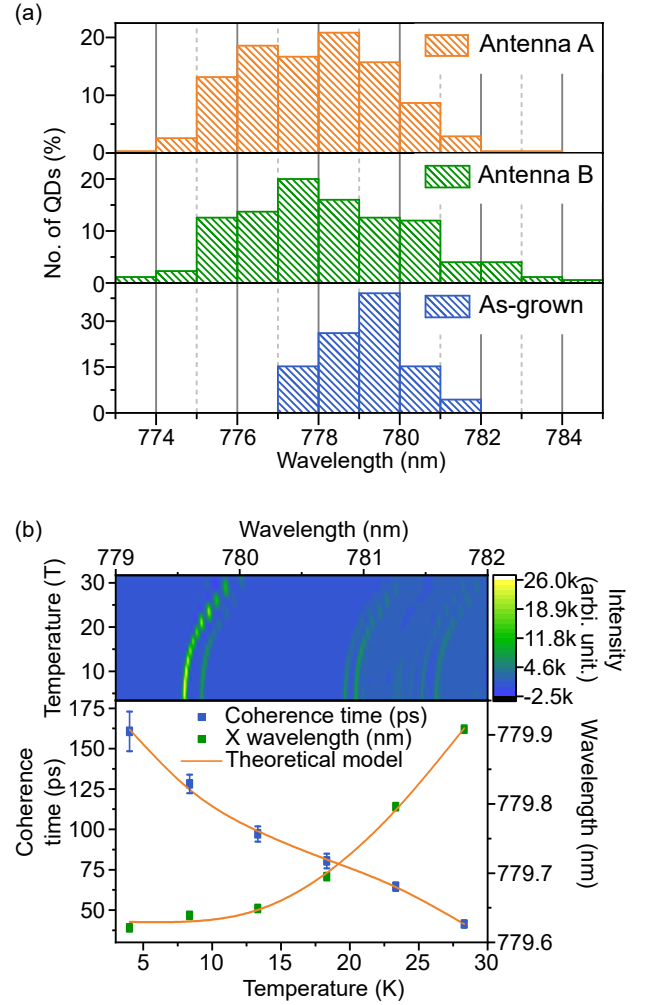


FIG. 1. Emission wavelength characteristics and tuning. (a) Statistics of the emission wavelength in fabricated dielectric antenna structures A (orange) and B (green), compared to the as-grown sample (blue), revealing only a slight change after fabrication. (b) Tuning of QD emission characteristics via temperature, revealing simultaneous changes in emission wavelength, intensity, and coherence time. Photoluminescence spectra (top) and coherence time of the neutral X photons (bottom) under off-resonant excitation for different temperatures.

a randomized phase [37]. This phase can be determined by measuring the detection events of the XX and X photon from each emission and therefore obtaining t . However, it is important to note that these types of time-resolved measurements are accompanied by a significant loss in overall efficiency for any protocol that relies on Bell state measurements (BSMs) with photons from different sources, such as quantum teleportation or entanglement swapping [38]. This even accounts for experiments using photon pairs emitted by the same source but at different times. Let us consider an emission process of entangled pairs from two separate devices with subsequent detection events in an entanglement swapping scheme as illustrated in fig. 2(b). Each emission from device A or B therefore

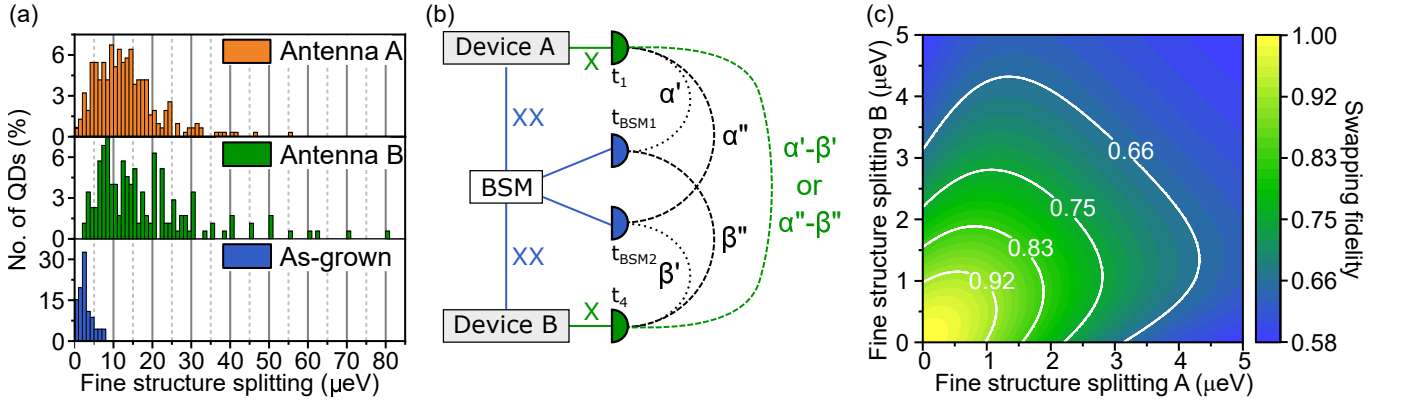


FIG. 2. Exciton fine structure characteristics and influence on entanglement swapping. (a) Statistics of the X fine structure splitting in fabricated dielectric antenna structures A (orange) and B (green), compared to the as-grown sample (blue), revealing a significant broadening of the distribution after fabrication. (b) Scheme of entanglement swapping using QDs with finite exciton fine structure. The phases in the entangled states emitted by device A and B are not accessible via measuring detection times. Two possible solutions arise (α', β' and α'', β''), leading to two swapped states in a statistical superposition with the phases $\alpha' - \beta'$ and $\alpha'' - \beta''$, which cannot be experimentally distinguished. (c) Fidelity of an entanglement swapping scheme with ideal quantum interference at the Bell state measurement (BSM), assuming finite exciton fine structure of two separate QDs and an exciton lifetime of 300 ps.

carries its respective phase factor $\alpha = -\frac{S_A}{\hbar}t_A$ or $\beta = -\frac{S_B}{\hbar}t_B$

$$|\psi_{1234}(\alpha, \beta)\rangle = \frac{1}{2}(|H_1H_2\rangle + e^{i\alpha}|V_1V_2\rangle)(|H_3H_4\rangle + e^{i\beta}|V_3V_4\rangle) \quad (2)$$

After projecting photons 2 and 3 on the Bell state $|\Psi_{2,3}^-\rangle = \frac{1}{\sqrt{2}}(|H_2V_3\rangle - |V_2H_3\rangle)$ one obtains the un-normalized state

$$|\psi_{1,4}(\alpha, \beta)\rangle = \langle\Psi_{2,3}^-|\psi_{1234}(\alpha, \beta)\rangle = e^{i\beta}(|H_1V_4\rangle - e^{i(\alpha-\beta)}|V_1H_4\rangle) \quad (3)$$

which means that similar to the case of entangled pair emission from a single device, the final (swapped) state is oscillating between two Bell states, here with the phase $\alpha - \beta$. In order to utilize this state, this phase has to be an experimentally accessible parameter. This is, however, not the case, since the BSM removes the 'which path' information, making it impossible to determine from which source each photon originated. Therefore, two possible combinations of phase factors are possible:

$$\alpha' = -\frac{S_A}{\hbar}(t_1 - t_{BSM1}) \quad \text{and} \quad \beta' = -\frac{S_B}{\hbar}(t_4 - t_{BSM2}) \quad (4)$$

or

$$\alpha'' = -\frac{S_A}{\hbar}(t_1 - t_{BSM2}) \quad \text{and} \quad \beta'' = -\frac{S_B}{\hbar}(t_4 - t_{BSM1}) \quad (5)$$

where the indices $i = 1, 4$ in t_i correspond to the photons described in the state $|\psi_{1234}\rangle$, and the $i = (BSM1), (BSM2)$ correspond to the photons detected at the two respective detectors of a BSM. Independent of the present fine structure splittings it is impossible to experimentally determine which of the two cases occurs and therefore which of the two states

$$|\psi_{1,4}(\alpha', \beta')\rangle \neq |\psi_{1,4}(\alpha'', \beta'')\rangle \quad (6)$$

is present. The final state is therefore not a coherent, but a statistical superposition of the two possible states $|\psi_{1,4}(\alpha', \beta')\rangle$ and $|\psi_{1,4}(\alpha'', \beta'')\rangle$. The entanglement of the swapped state only persists in the case of low X fine structure splittings and radiative decay times or the case of $t_{BSM,1} = t_{BSM,2}$. The latter case is undesirable since it strongly lowers the efficiency of the BSM by discarding many detection events $t_{BSM,1} \neq t_{BSM,2}$ within the coincidence window. A finite FSS in separate devices significantly lowers the fidelity of the two-photon states obtained in an entanglement swapping scheme, as illustrated in 2(c) under the assumption of perfect quantum interference at the Bell state measurement. Therefore, a scalable application of QD based entangled photon sources relies on tuning the fine structure and removing the state oscillation, e.g., via frequency-shifting optical setups [39, 40] or external fields such as anisotropic strain. Once such tuning is realized with high efficiency it allows for strong pair-wise photonic entanglement from individual QDs which can then be applied in quantum networks.

IV. NETWORK-RELEVANT DEVICE CHARACTERISTICS

In the next step, one QD from each device (antenna A and B) is selected and the temperature of antenna B adjusted to 10.81 K, thereby realizing the overlap of XX transitions between the two independent QDs from each device. We now investigate the differences in the parameters required for an entanglement swapping scheme. Figures 3(a-c) show the relevant properties for quantum interference, i.e. the BSM in entanglement swapping, and figures. 3(d-f) for entanglement of the initial pair-wise entanglement. To efficiently excite the XX state, two-photon excitation is performed on the two QDs in the devices by using a π -pulse. Due to slight differences in XX binding energies (in our case ≈ 0.26 meV) the X and XX transitions cannot be perfectly tuned in resonance with

each other simultaneously. Figure 3(a) illustrates the intensity auto-correlation $g^{(2)}(\tau)$ from the XX streams of device A and B. At zero time delay, $g_A^2(0) = g_B^2(0) \approx 0.03$ is determined, indicating a high single-photon purity and negligible effect on quantum interference [41] between photons from the two devices. Apart from that, the data is superimposed by a bunching towards zero time delay, giving evidence to blinking. Such emission intermittence [42] can be explained by residual charges in the QD blocking the resonant excitation of the neutral XX. The "on"-fractions are $46.9(3) \pm 0.42\%$ and $51.1(2) \pm 0.83\%$ for device A and B (see supplementary), respectively [43]. Blinking [44, 45] is detrimental for the efficiency of quantum interference [46] (in our case estimated to $48.9(4)\%$) and therefore also entanglement swapping.

The success of quantum interference is furthermore governed by the photon indistinguishability of each photon source, typically determined by $V_{\delta E} = T_2/2T_1$. Figures 3(b) and (c) show the lifetime and coherence time measurements from the XX photons of each device. The indistinguishabilities are therefore estimated to $V_{\delta E}^{(XXA)} = 34.0(0)\%$ and $V_{\delta E}^{(XXB)} = 26.4(4)\%$, respectively. The limited coherence is usually attributed to dephasing due to charge and spin noise or phonon scattering [47]. The ratio of the lifetimes of XX and X (i.e. $0.67(3)$ for QD in device B) is limiting the indistinguishability even further (in our case to $\sim 15.7\%$) due to intrinsic dephasing in the cascade emission [28]. A shortening of XX lifetime, e.g. by the Purcell effect, is therefore beneficial for addressing both discussed points that limit the indistinguishability simultaneously [27, 28, 48].

The experimentally relevant degree of entanglement is determined by the X fine structure splitting, radiative lifetime, and spin scattering times. In the GaAs/AlGaAs material system, QDs can be found where spin scattering has only a small influence in the GaAs/AlGaAs material system [34]. The X lifetime measurement of device B is shown in fig. 3(d). Although a lower X lifetime would lead to less phase noise in the entangled state, it deteriorates quantum interference visibilities at the same time, and therefore the success of BSM required in the entanglement swapping scheme.

The QD in device B exhibits a fine structure splitting of $4.22(8)\mu\text{eV}$. The polarization entanglement is obtained by polarization-resolved cross-correlation measurements and quantum tomography. Gating of detection events can be applied to enhance the measured degree of entanglement at the expense of coincidence counts [25]. This relationship is displayed in fig 3(e). The fidelity of the entanglement can be strongly enhanced when the gate-time window size is reduced to 500 ps. The corresponding real part of the two-photon density matrix is shown in fig 3(f) (imaginary part shown in supplementary). However, the coincidence counts also decrease significantly.

Time-gating can also lead to the improved success of BSMs in entanglement swapping [25], also with the expense of reduced overall coincidences. The efficiency of entanglement swapping, i.e. the four-fold coincidence detection rate, is furthermore determined by the source efficiency, including the excitation and collection efficiency as well as the coupling ef-

ficiency into a single-mode fiber which depends on the mode profile of the emission.

We can eventually identify all parameters that are statistically distributed in the QD devices, which affect the entanglement swapping using polarization-entangled photon pairs from different devices, generated using the XX-X cascade:

- Exciton emission wavelength
- Exciton fine structure splitting
- Exciton lifetime
- Biexciton lifetime
- Exciton spin scattering time
- Pure dephasing time
- Total efficiency (including excitation, collection, fiber coupling)

Although the pure dephasing times may be different for XX and X emission, we assume it to be identical here, since both transitions are affected by dephasing due to the solid-state environment in a similar way. For actual networks of multiple sources or coupling to quantum memories, the binding energy of the XX also plays a role and is statistically distributed, but is not mentioned in the list above.

V. PREDICTIONS FOR A REAL-WORLD QUANTUM NETWORK

We now develop a theoretical model which takes into account the statistical effect on the fidelity of photons that result from entanglement swapping. The first prerequisite is the overlap of the emission wavelengths between two independent sources. To estimate that, first the probability density of finding a QD with a specific wavelength in device A and B is obtained (based on fig. 1) and shown in 4(a). Under the assumption that the probability density of the emission wavelengths obeys a standard distribution, we can describe it by

$$p(\lambda) = \frac{1}{\sqrt{2\pi}\sigma} \cdot e^{-\frac{(\lambda-\mu)^2}{2\sigma^2}} \quad (7)$$

where $p(\lambda)$ is the probability density, μ, σ are the expected and standard deviation values of the distribution. By fitting the data it is possible to extract the corresponding values (see supplementary). Next, the tuning range for the employed wavelength tuning of each device δ_λ is defined. Now we can analytically calculate the probability of tuning two devices into resonance (see supplementary). Figure 4(b) shows the result, assuming an equal σ_λ in the devices, but different expected values with a difference of $\Delta\mu_\lambda$. Here, an exemplary wavelength tuning range of 1 nm for each device is assumed. The color-map shows that high probability can be obtained with a decreasing expected value difference $\Delta\mu_\lambda$ and narrower wavelength standard deviation σ_λ . Furthermore, for higher $\Delta\mu_\lambda$ and a fixed tuning range, it is beneficial to have σ_λ that is not

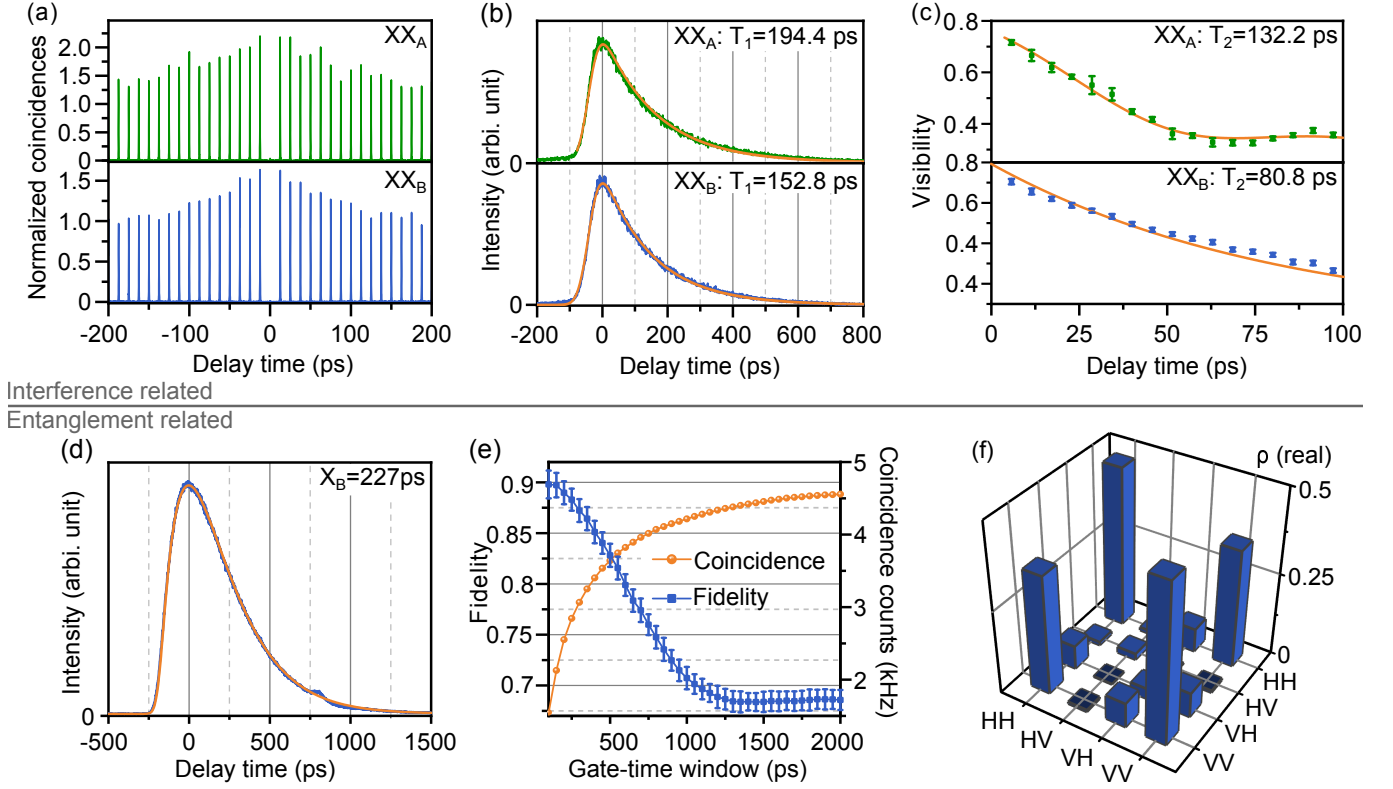


FIG. 3. Optical properties from separate devices required for efficient entanglement swapping. (a-c) Quantum interference-related properties of the XX photons from two devices (A and B) that have been tuned into resonance via temperature tuning. (a) Second-order autocorrelation measurements for the XX photons streams of both devices, revealing pure single-photon emission as well as blinking. (b) Lifetime measurements and (c) coherence time measurements of both XX photon streams. (d-f) Entanglement-related properties of the QD in device B. (e) Entanglement fidelity and raw coincidence counts, obtained via quantum tomography based on polarization-resolved cross-correlation measurements between XX and X emissions, as a function of gate-time window size. (f) Real part of the two-photon density matrix obtained at a gate window size of 500 ps.

too small, in order to increase the chance of tuning remote devices into resonance.

The model is now extended further, in order to obtain the fidelity of the swapped photon pairs based on the statistically distributed parameters in the devices. The exact nature of the distribution is not clear for every parameter and can be adapted for each specific QD material and fabricated device. Here we assume that the probability density for all parameters (e.g. X fine structure splitting) follows a (truncated) Gaussian distribution. This assumption models the fine structure well, as can be seen in fig. 4(a). The rest of the parameters were approximated by reasonable experimental values (see supplementary) based on the presented experiments and the existing literature. X spin scattering times are not considered here, as there is very little solid information on their distribution for each QD. Also, the total efficiency of each device and limited single-photon purities are considered independently of the theoretical model.

The model is based on a numerical approach. First, a random set of parameters is drawn for each parameter from device A and B. A tuning mechanism can now be considered which e.g. tunes the wavelengths from the different devices into resonance, potentially also affecting the other parameters.

Then, the swapping fidelity is analytically calculated. This process of random sampling is repeated one million times. The resulting fidelities of the swapped state are then normalized to display a probability density. Figure 4(c) shows the resulting probability distribution for obtaining a certain entanglement swapping fidelity for several considered cases. The integration of the probability density within a certain fidelity range then can yield the total probability for obtaining a fidelity within this range in a swapping experiment. Here, we consider a BSM with polarizing beam splitters, which is known to result in a lower limit of 0.5 in the swapping fidelity [25]. This coincides with the upper fidelity limit for classical two-photon states. Since we do not consider spin-scattering or limited single-photon purity here, the swapped fidelities will not fall below 0.5. The blue curve (1) shows the probability density considering the experimental parameters obtained in this work and assuming temperature tuning. It is clear that entanglement swapping is mostly not successful, leading to fidelities close to 0.5. The reason is the limited tuning range via temperature and the simultaneous decrease in photon coherence. For the orange curve (2) we now assume that all QDs from both devices can be tuned into resonance with each other (e.g. by strain tuning) without affecting other proper-

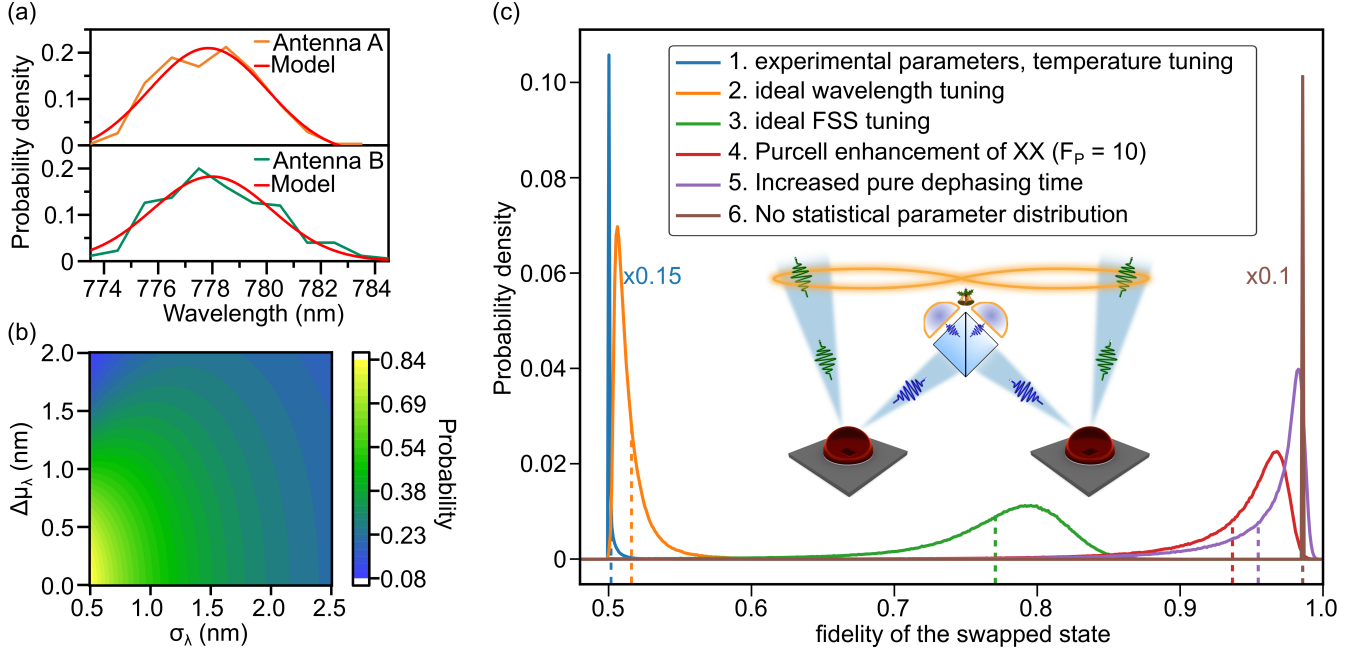


FIG. 4. Estimated device performance in a quantum network based on entanglement swapping. The properties of individual QDs are defined by probability density distributions as exemplarily shown in (a) for the emission wavelengths from device A and B. The experimental data is fitted with a Gaussian curve. Other properties (FSS, T_1 , T_2 , not shown) are modeled by truncated Gaussian distributions. (b) Probability for tuning the emission wavelength of two randomly selected QDs from separate devices into resonance, assuming a wavelength tuning range of $\delta_\lambda = 1$ nm. The emission wavelength standard deviation σ_λ is set equal for both devices, while the expected value has a difference of $\Delta\mu_\lambda$. (c) Probability density of the entanglement fidelity after swapping entanglement between photon pairs emitted by separate devices. The semi-analytical model incorporates a random sampling of experimentally reasonable QD property distributions from both devices. One million samples are used to obtain the probability density. The blue line (curve 1) shows the fidelity distribution for the experimentally accessed parameters in this work. Possible improvements in the fidelity distribution by consecutively adding tuning mechanisms and optimizing device properties are shown in curves 2 to 5. Curve 6 shows the case with removed statistical parameter distribution.

ties. This leads to a visible increase of entanglement fidelity. However, the values are still located mostly below 0.6. The reason is the X fine structure in the devices. Therefore we assume an additional tuning mechanism for the fine structure (e.g. anisotropic strain tuning) with a magnitude of $50\mu\text{eV}$. The resulting green curve (3) now shows fidelities between 0.75 and 0.85. If furthermore a selective Purcell enhancement of the XX emission with a Purcell factor of $F_P = 10$ is added [49], the red curve (4) arises. Another significant increase in entanglement swapping fidelity is the result, with fidelities ranging between 0.85 and 0.97. To increase the probability of a high swapping fidelity, even more, the pure dephasing times can be significantly increased. The result is shown by the violet curve (5), exhibiting fidelities between 0.9 and 0.99. Curve (6) shows the comparison to the expected probability density if the parameters would not be statistically distributed at all. Therefore the statistical effect of QD properties on entanglement swapping is clear by comparing curves (5) and (6). Only a very small chance exists, that two QDs can be found such that the swapped fidelity is actually above those of curve (6). Due to the distribution of properties, the swapped entanglement deteriorates in almost all cases. How much lower the fidelity becomes is directly related to the relative uncertainties in the distributed parameters. Now the question has to be raised where the advantage in using QD-based entangled

photon sources lies. In comparison to commonly employed SPDC sources, QDs allow for a deterministic emission of photon pairs. However, to really offer an advantage over SPDC sources, QD-based sources must show better total efficiencies while offering the same possible fidelities of swapped photon pairs. This fidelity can be very high for SPDC sources [50]. For QD-based sources to achieve these fidelities, material growth and device fabrication have to be controlled to an extent that allows for highly narrow distributions in optical properties. Tuning methods of emission wavelength and fine structure are required. Simultaneously, QDs may need to be embedded in devices suppressing blinking and increasing coherence.

VI. CONCLUSION

We present insights on the scalability of semiconductor-enabled quantum photonic networks based on experimental observations and a developed numerical model. Considering QD-based dielectric optical antennas in an entanglement swapping scheme serves as an example for unraveling the challenges for employing semiconductor QDs in applications such as quantum repeaters. We showed that the exciton fine structure is detrimental for scalable networks and therefore re-

quires tuning. The statistical distribution of parameters (e.g. emission wavelengths and fine structures) in two separate devices are studied, and the influence on the achievable entanglement swapping fidelities investigated. Two QDs from the separate devices are tuned into resonance with each other by temperature tuning, and the properties of the single and entangled photon characteristics are evaluated.

Different tuning techniques are contemplated, revealing that the desired tuning of one parameter is often accompanied by a simultaneous tuning of others. Anisotropic strain tuning is most promising for independent tuning of independent parameters (i.e. wavelength and fine structure). Further challenges such as blinking and limited coherence can be addressed e.g. by implementing QD devices with dynamic charge tuning [51]. A selective Purcell enhancement of the XX emission can be obtained using circular Bragg gratings [20]. However, the combination of all 3 techniques is technologically very demanding. In addition, since a large parameter space exists for generating polarization-entangled photon pairs from the XX-X cascade, not all important parameters can be tuned deterministically. A random sampling of several properties is thus unavoidable, posing intensified requirements to the material growth in order to obtain scalable semiconductor devices. Deviation of device parameters may necessitate entanglement purification, which uses up available resources in a quantum network and therefore may relativize the key advantage of source efficiency of QD-based sources. Therefore the level of control over the parameter statistics directly translates to a potential advantage of QD-based sources in a quantum network. A possible alternative is to generate photonic en-

tanglement with a significantly larger number of photons per individual QD first (e.g. cluster states) [21], before interfacing with photons from other sources.

This discussion and the numerical prediction can easily be extended to other types of solid-state quantum light emitters or quantum memories with photon interfaces (comprising entanglement generation via photon interference). The model incorporates well-known analytical approaches for the independent physical problems (entangled two-photon states for individual QDs and subsequent entanglement swapping) whereas a numerical solution based on random sampling serves to evaluate the influence of statistical distributions of parameters in the chosen material system. This distribution eventually leads to the degradation of remote entanglement, necessitating time gating or correction protocols like entanglement purification which reduce the overall quantum network efficiency. It is therefore a key challenge for the scalable implementation of solid-state quantum light sources.

ACKNOWLEDGMENTS

The authors gratefully acknowledge the funding by the German Federal Ministry of Education and Research (BMBF) within the project Q.Link.X (16KIS0869), the funding by the European Research Council (QD-NOMS GA715770) and the Deutsche Forschungsgemeinschaft (DFG, German Research Foundation) under Germany's Excellence Strategy – EXC-2123 Quantum Frontiers – 390837967.

-
- [1] A. Zeilinger, *Phys. Scripta* **T76**, 203 (1998).
 - [2] M. Pant, H. Krovi, D. Towsley, L. Tassiulas, L. Jiang, P. Basu, D. Englund, and S. Guha, *npj Quantum Inf.* **5** (2019).
 - [3] F. B. Basset, M. Valeri, E. Roccia, V. Muredda, D. Poderini, J. Neuwirth, N. Spagnolo, M. B. Rota, G. Carvacho, F. Sciarrino, and R. Trotta, *Sci Adv* **7**, eabe6379 (2021).
 - [4] H.-S. Zhong, H. Wang, Y.-H. Deng, M.-C. Chen, L.-C. Peng, Y.-H. Luo, J. Qin, D. Wu, X. Ding, Y. Hu, P. Hu, X.-Y. Yang, W.-J. Zhang, H. Li, Y. Li, X. Jiang, L. Gan, G. Yang, L. You, Z. Wang, L. Li, N.-L. Liu, C.-Y. Lu, and J.-W. Pan, *Science* **370**, 1460 (2020).
 - [5] J.-G. Ren, P. Xu, H.-L. Yong, L. Zhang, S.-K. Liao, J. Yin, W.-Y. Liu, W.-Q. Cai, M. Yang, L. Li, K.-X. Yang, X. Han, Y.-Q. Yao, J. Li, H.-Y. Wu, S. Wan, L. Liu, D.-Q. Liu, Y.-W. Kuang, Z.-P. He, P. Shang, C. Guo, R.-H. Zheng, K. Tian, Z.-C. Zhu, N.-L. Liu, C.-Y. Lu, R. Shu, Y.-A. Chen, C.-Z. Peng, J.-Y. Wang, and J.-W. Pan, *Nature* **549**, 70 (2017).
 - [6] Q.-C. Sun, Y.-L. Mao, Y.-F. Jiang, Q. Zhao, S.-J. Chen, W. Zhang, W.-J. Zhang, X. Jiang, T.-Y. Chen, L.-X. You, L. Li, Y.-D. Huang, X.-F. Chen, Z. Wang, X. Ma, Q. Zhang, and J.-W. Pan, *Phys. Rev. A* **95**, 032306 (2017).
 - [7] P. G. Kwiat, *Science* **290**, 498 (2000).
 - [8] E. Megidish, A. Halevy, T. Shacham, T. Dvir, L. Dovrat, and H. S. Eisenberg, *Phys. Rev. Lett.* **110**, 210403 (2013).
 - [9] Y. Zhang, Z. Chen, S. Pirandola, X. Wang, C. Zhou, B. Chu, Y. Zhao, B. Xu, S. Yu, and H. Guo, *Phys. Rev. Lett.* **125**, 010502 (2020).
 - [10] U. L. Andersen, J. S. Neergaard-Nielsen, P. van Loock, and A. Furusawa, *Nat. Phys.* **11**, 713 (2015).
 - [11] Y. Chen, J. Zhang, M. Zopf, K. Jung, Y. Zhang, R. Keil, F. Ding, and O. G. Schmidt, *Nat Commun* **7**, 1 (2016).
 - [12] V. Giesz, S. L. Portalupi, T. Grange, C. Antón, L. D. Santis, J. Demory, N. Somaschi, I. Sagnes, A. Lemaître, L. Lanco, A. Auffèves, and P. Senellart, *Phys. Rev. B* **92**, 161302 (2015).
 - [13] D. Bouwmeester, J.-W. Pan, K. Mattle, M. Eibl, H. Weinfurter, and A. Zeilinger, *Nature* **390**, 575 (1997).
 - [14] J.-W. Pan, D. Bouwmeester, H. Weinfurter, and A. Zeilinger, *Phys. Rev. Lett.* **80**, 3891 (1998).
 - [15] J.-W. Pan, Z.-B. Chen, C.-Y. Lu, H. Weinfurter, A. Zeilinger, and M. Żukowski, *Rev. Modern Phys.* **84**, 777 (2012).
 - [16] V. Scarani, H. de Riedmatten, I. Marcikic, H. Zbinden, and N. Gisin, *Eur. Phys. J. D* **32**, 129 (2004).
 - [17] P. Senellart, G. Solomon, and A. White, *Nat. Nanotechnology* **12**, 1026 (2017).
 - [18] H. Wang, Y.-M. He, T.-H. Chung, H. Hu, Y. Yu, S. Chen, X. Ding, M.-C. Chen, J. Qin, X. Yang, *et al.*, *Nat. Photonics* **13**, 770 (2019).
 - [19] R. M. Stevenson, R. J. Young, P. Atkinson, K. Cooper, D. A. Ritchie, and A. J. Shields, *Nature* **439**, 179 (2006).
 - [20] J. Liu, R. Su, Y. Wei, B. Yao, S. F. C. da Silva, Y. Yu, J. Iles-Smith, K. Srinivasan, A. Rastelli, J. Li, and X. Wang, *Nat. Nanotechnology* **14**, 586 (2019).
 - [21] I. Schwartz, D. Cogan, E. R. Schmidgall, Y. Don, L. Gantz, O. Kenneth, N. H. Lindner, and D. Gershoni,

- Science* **354**, 434 (2016).
- [22] M. Kroutvar, Y. Ducommun, D. Heiss, M. Bichler, D. Schuh, G. Abstreiter, and J. J. Finley, *Nature* **432**, 81 (2004).
 - [23] P. van Loock, W. Alt, C. Becher, O. Benson, H. Boche, C. Deppe, J. Eschner, S. Höfling, D. Meschede, P. Michler, *et al.*, *Adv Quantum Technol* **3**, 1900141 (2020).
 - [24] L.-K. Chen, H.-L. Yong, P. Xu, X.-C. Yao, T. Xiang, Z.-D. Li, C. Liu, H. Lu, N.-L. Liu, L. Li, T. Yang, C.-Z. Peng, B. Zhao, Y.-A. Chen, and J.-W. Pan, *Nat. Photonics* **11**, 695 (2017).
 - [25] M. Zopf, R. Keil, Y. Chen, J. Yang, D. Chen, F. Ding, and O. G. Schmidt, *Phys. Rev. Lett.* **123**, 160502 (2019).
 - [26] M. B. Rota, F. B. Basset, D. Tedeschi, and R. Trotta, *IEEE J SEL TOP QUANT* **26**, 1 (2020).
 - [27] C. Schimpf, M. Reindl, F. Basso Basset, K. D. Jöns, R. Trotta, and A. Rastelli, *Appl. Phys. Lett.* **118**, 100502 (2021).
 - [28] E. Schöll, L. Schweickert, L. Hanschke, K. D. Zeuner, F. Sbresny, T. Lettner, R. Trivedi, M. Reindl, S. F. C. da Silva, R. Trotta, *et al.*, *Phys. Rev. Lett.* **125**, 233605 (2020).
 - [29] Y. Chen, M. Zopf, R. Keil, F. Ding, and O. G. Schmidt, *Nat Commun* **9**, 1 (2018).
 - [30] J. Yang, C. Nawrath, R. Keil, R. Joos, X. Zhang, B. Höfer, Y. Chen, M. Zopf, M. Jetter, S. L. Portalupi, F. Ding, P. Michler, and O. G. Schmidt, *Opt. Express* **28**, 19457 (2020).
 - [31] F. B. Basset, M. B. Rota, C. Schimpf, D. Tedeschi, K. D. Zeuner, S. C. Da Silva, M. Reindl, V. Zwiller, K. D. Jöns, A. Rastelli, *et al.*, *Phys. Rev. Lett.* **123**, 160501 (2019).
 - [32] J. H. Weber, B. Kambs, J. Kettler, S. Kern, J. Maisch, H. Vural, M. Jetter, S. L. Portalupi, C. Becher, and P. Michler, *Nat. Nanotechnology* **14**, 23 (2018).
 - [33] M. Bayer, G. Ortner, O. Stern, A. Kuther, A. Gorbunov, A. Forchel, P. Hawrylak, S. Fafard, K. Hinzer, T. Reinecke, *et al.*, *Phys. Rev. B* **65**, 195315 (2002).
 - [34] R. Keil, M. Zopf, Y. Chen, B. Höfer, J. Zhang, F. Ding, and O. G. Schmidt, *Nat Commun* **8**, 1 (2017).
 - [35] D. J. P. Ellis, R. M. Stevenson, R. J. Young, A. J. Shields, P. Atkinson, and D. A. Ritchie, *Appl. Phys. Lett.* **90**, 011907 (2007).
 - [36] A. Muller, W. Fang, J. Lawall, and G. S. Solomon, *Phys. Rev. Lett.* **103**, 217402 (2009).
 - [37] R. Winik, D. Cogan, Y. Don, I. Schwartz, L. Gantz, E. R. Schmidgall, N. Livneh, R. Rapaport, E. Buks, and D. Gershoni, *Phys. Rev. B* **95**, 235435 (2017).
 - [38] M. Anderson, T. Müller, J. Huwer, J. Skiba-Szymanska, A. Krysa, R. Stevenson, J. Heffernan, D. Ritchie, and A. Shields, *npj Quantum Inf* **6**, 1 (2020).
 - [39] X.-B. Wang, C.-X. Yang, and Y.-B. Liu, *Appl. Phys. Lett.* **96**, 201103 (2010).
 - [40] A. Fognini, A. Ahmadi, S. J. Daley, M. E. Reimer, and V. Zwiller, *Opt. Express* **26**, 24487 (2018).
 - [41] H. Ollivier, S. Thomas, S. Wein, I. M. de Buy Wenniger, N. Coste, J. Lored, N. Somaschi, A. Harouri, A. Lemaitre, I. Sagnes, L. Lanco, C. Simon, C. Anton, O. Krebs, and P. Senellart, *Phys. Rev. Lett.* **126**, 063602 (2021).
 - [42] J.-P. Jahn, M. Munsch, L. Béguin, A. V. Kuhlmann, M. Renggli, Y. Huo, F. Ding, R. Trotta, M. Reindl, O. G. Schmidt, A. Rastelli, P. Treutlein, and R. J. Warburton, *Phys. Rev. B* **92**, 245439 (2015).
 - [43] H. S. Nguyen, G. Sallen, M. Abbarchi, R. Ferreira, C. Voisin, P. Roussignol, G. Cassabo, and C. Diederichs, *Phys. Rev. B* **87**, 115305 (2013).
 - [44] C. Hopfmann, W. Nie, N. L. Sharma, C. Weigelt, F. Ding, and O. G. Schmidt, *Phys. Rev. B* **103**, 075413 (2021).
 - [45] C. Hopfmann, N. L. Sharma, W. Nie, R. Keil, F. Ding, and O. G. Schmidt, *Phys. Rev. B* **104**, 075301 (2021).
 - [46] K. D. Jöns, K. Stensson, M. Reindl, M. Swillo, Y. Huo, V. Zwiller, A. Rastelli, R. Trotta, and G. Björk, *Phys. Rev. B* **96**, 075430 (2017).
 - [47] L. Zhai, G. N. Nguyen, C. Spinnler, J. Ritzmann, M. C. Löbl, A. D. Wieck, A. Ludwig, A. Javadi, and R. J. Warburton, *arXiv preprint arXiv:2106.03871* (2021).
 - [48] T. Huber, A. Predojević, H. Zoubi, H. Jayakumar, G. S. Solomon, and G. Weihs, *Opt. Express* **21**, 9890 (2013).
 - [49] H. Wang, H. Hu, T.-H. Chung, J. Qin, X. Yang, J.-P. Li, R.-Z. Liu, H.-S. Zhong, Y.-M. He, X. Ding, *et al.*, *Phys. Rev. Lett.* **122**, 113602 (2019).
 - [50] C. Zhang, Y.-F. Huang, C.-J. Zhang, J. Wang, B.-H. Liu, C.-F. Li, and G.-C. Guo, *Opt. Express* **24**, 27059 (2016).
 - [51] L. Zhai, M. C. Löbl, G. N. Nguyen, J. Ritzmann, A. Javadi, C. Spinnler, A. D. Wieck, A. Ludwig, and R. J. Warburton, *Nat Commun* **11**, 1 (2020).